11TH INTERNATIONAL SCIENTIFIC CONFERENCE ON DEFENSIVE TECHNOLOGIES
OTEH 2024
Serbia, Tara, 9-11 October 2024

DESIGN AND EXPERIMENTAL EVALUATION OF A MISSILE LATERAL THRUSTER

TOUFIK ALLOUCHE
University of Defence – Military Academy, Belgrade, toufik.allouche@gmail.com

SAŠA ŽIVKOVIĆ
Military Technical Institute, Belgrade, sasavite@yahoo.com

MARKO KARIĆ
Military Technical Institute, Belgrade, karicmarko83@gmail.com

ABDELLAH FERFOURI
University of Defence Belgrad; Military Academy fer-abdel@hotmail.com

DAMIR JERKOVIĆ
University of Defence Belgrad; Military Academy damir.d.jerkovic@gmail.com

NEBOJŠA HRISTOV
University of Defence Belgrad; Military Academy, nebojsahristov@gmail.com

Abstract: *Lateral thrusters are small, short-duration rocket motor mounted on the lateral side of the missile to provide a force able to change the missile's direction. In the present paper, a design and experimental evaluation of a solid propellant thruster is considered. The design starts from technical requirements, internal ballistic calculation, thruster prototype manufacturing and finally static tests on a static test bench to evaluate its internal pressure profile. In design, the propellant imperfections are considered. After tests and simulations, a comparative analysis between the analytical and the experimental results is done.*

Keywords: *Side thruster, solid rocket motor design, internal ballistic, static tests, missile control system.*

1. INTRODUCTION

For guided missiles, control systems based on aerodynamic control surfaces present some physical limitations, particularly at low speed and at high altitudes where the air density is low. To improve maneuverability and overcome these limitations, thrusters are a very good addition which offer better agility, maneuverability as well as a much faster response time to the commands. For achieving higher precision, lower cost and better manoeuvrability, this alternative method of control has been integrated into several areas of missile systems as the trajectory tracking on artillery, or course refining on air defense intercepters as shown in Figure 1.

Figure 1. (a) Missile R624 [1] , (b) Control section of PAC-3 [2]

Thrusters are small solid rocket, short-duration, high-force motor mounted in the lateral side of the missile to provide a force able to change/reorient the missile's direction. The thruster is composed of a metal structure (casing with an insulation), an igniter, a grain (solid propellant) and a nozzle as shown in Figure 2.

In missile systems, thrusters can be used in several areas of application, namely: Trajectory tracking [3,4], Anti-ballistic and air defense interceptors [5] and Anti-tank rockets [6].

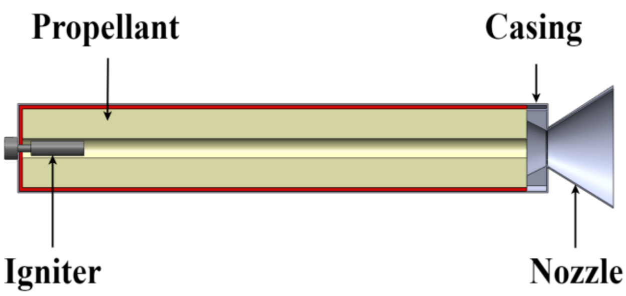

Figure 2. Components of solid rocket motor

The process of solid rocket motor design requires first to determine application field, input data as the thrust

Corresponding author: T.Allouche;
E-mail: lab@trzk.co.rs
DOI: 10.5937/OTEH24006A

(generated force), burning time and the total impulse then comes the second step where the propellant grain design and the propellant properties are chosen in such way that they respond to requierements. Numerical calculation allow to predict the thruster's performances.

In the field of SPRM (Solid Propellant Rocket Motor) design, significant researches are done and scientific papers are published; this concerns the design of the motor casing [7-9], grain propellant [10,11], experimental performance tests [12,13]. There are also works that encompass more than one aspect [14,15].

2. EXPERIMENTAL BENCH

The experimental part consists to conduct a static test on the designed motor in order to evaluate the pressure profile. These tests are essential to validate the theoritical curve predicted by the analytical model. Figure 3. presents a schema of the test bench used to measure the pressure of the combustion chamber of the motor using an adequate presssure transducer.

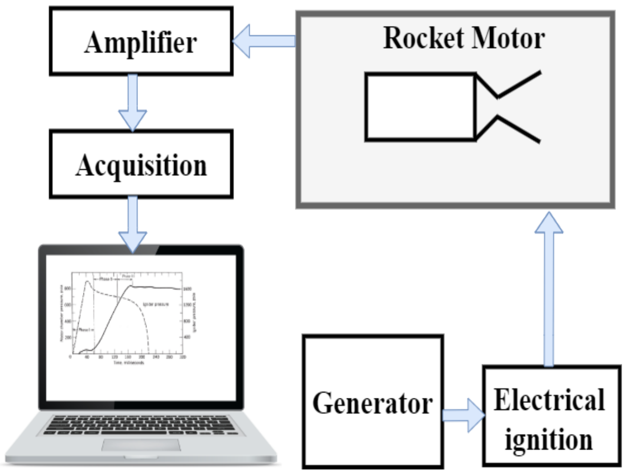

Figure 3. Experimental test bench

The test bench is composed of 3 systems: Motor installation, power alimentation, acquisition and processing.

- Motor installation: composed of a thruster prototype, a support where the thruster is fixed, a pressure transducer connected to combustion pressure and an electrical igniter.
- Power alimentation: the electric device needed to generate the ignition current as well as the control box and the associated wiring.
- Acquisition and processing: composed of an amplifier, an acquisition device and a laptop to process and display data.

3. ANALYTICAL CALCULATION

3.1. Flight requirements

Thrusters are employed to deliver a short-duration impulse then, the thruster must use a quick-burn propellant, this propellant has the ability to generate thrust in short operating time of the order of few milliseconds. For that:

- The propellant shown in table 1. is chosen;
- A multi-tubes propellant configuration with internal-external burning is chosen.

The propellant presented in Table 1 is used.

Table 1. Propellant characteristics

Characteristics	Value	Unit
Density	1620	[Kg/m3]
Specific heat ratio	1.24	[/]
Temperature of combustion	2345	[K]
Molar mass	23.1	[Kg/Kmol]
Specific impulse	2000	[N.s/Kg]

The motor initial parameters are presented in Table 2.

Table 2. Motor characteristics

Characteristics	Value	Unit
Thrust force	600	[N]
Effective working time	10	[ms]
Internal pressure	125	[bar]
Throat diameter	3.5	[mm]

3.2. Internal ballistics equations

The motor's internal parameters are calculated using the internal ballistic mathematic model of rocket motors.

Solid propellant mass is defined as the ratio between the total impulse and the specific impulse of the propellant. It is given by equation (1):

$$m = \frac{F \cdot t_e}{I_{sp}} \tag{1}$$

The mass flow rate of combustion gases can be calculated with equation (2):

$$\dot{m} = \frac{m}{t_e} \tag{2}$$

Mass flow coefficient:

$$C_d = \sqrt{\frac{\kappa}{RT_0} \cdot \left(\frac{2}{k+1}\right)^{\frac{k+1}{k-1}}} \tag{3}$$

The exit diameter of nozzle is related to the throat diameter and the product gases characteristics. It is given by equation (4):

$$D_e = D_{th} \sqrt{\frac{\left(\frac{2}{\kappa+1}\right)^{\frac{1}{\kappa-1}} \cdot \left(\frac{P_0}{P_a}\right)^{\frac{1}{\kappa}}}{\sqrt{\frac{\kappa+1}{\kappa-1} \cdot \left[1 - \left(\frac{P_0}{P_a}\right)^{\frac{1-\kappa}{\kappa}}\right]}}} \tag{4}$$

Burning rate [16]:

$$r = a \cdot P^n \tag{5}$$

Burning rate at different initial propellant temperature:

$$r_{T_i} = r_{T_0} \cdot e^{\sigma \cdot (T_i - T_0)} \tag{6}$$

The pressure-time curve can be predicted solving the system of differential equations presented as follow:

$$\begin{gathered} \frac{d}{dt}P(t) = \frac{R \cdot T_0 \cdot A_b \cdot (t) \cdot r(t) \cdot \rho}{V_0(t)} - \frac{A_{th}}{V_0(t)} \sqrt{\kappa \cdot R \cdot T_0 \left(\frac{2}{\kappa+1}\right)^{\frac{\kappa+1}{\kappa-1}}} \cdot P(t) - \frac{A_b \cdot (t) \cdot r(t) \cdot P(t)}{V_0(t)} \\ \frac{d}{dt}x(t) = r(t) \end{gathered} \tag{7}$$

Combustion chamber free volume

$$V_0(t) = V_0(0) + \int_0^t A_b(t) \cdot r(t) dt \tag{8}$$

The thrust is defined as the product of the chamber pressure, the thrust coefficient and the throat area [16]:

$$F = C_F \cdot P \cdot A_{th} \tag{9}$$

The throat area is given by:

$$A_{th} = \frac{\pi \cdot D_{th}^2}{4} \tag{10}$$

3.3. Propellant grain configuration

The multi-tubes configuration of the propellant used in the thruster is described in Figure 4.

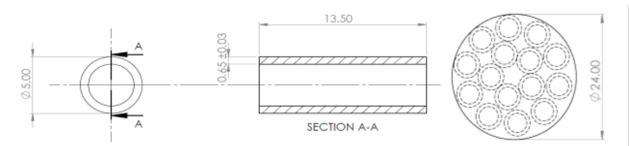

(a) (b)

Figure 4. (a) Unit tubular propellant geometry, (b) propellant configuration

The burning surface area for an ideal propellant unit tube is done by equation (10):

$$A_b(x) = 15 \cdot \left[2 * \frac{\pi}{4} \left[(D-2x)^2 - (d+2x)^2 \right] + \pi (L-2x) \cdot (D+d) \right] \tag{11}$$

The solid propellant is formed into the desired shape by extruding. The non-coaxiality tolerance of the extrusion machine is measured and equal to 0.1 mm. This inaccuracy in propellant manufacturing has an effect on the burning surface area so on the rocket motor's performances.

Table 3. Motor performances

Characteristics	Value	Unit
Mass of propellant	0.003	[Kg]
Mass flow	0.3	[Kg/s]
Mass flow coefficient	0.00071425	[/]
Thrust coefficient	1.45	[/]

Figure 5 presents the graphs of variations of the burning surface area as function of web distance for a grain of 15 ideal tubes and for a grain of 15 tubes with a non-coaxiality of 0.1mm.

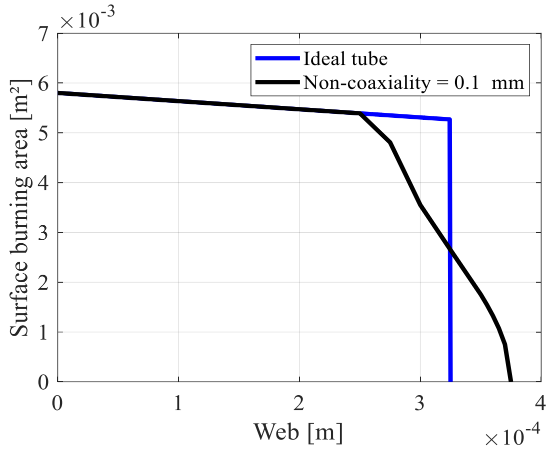

Figure 5. Total burning surface area versus web distance

3.4. Burning rate

Table 4. Burning rate r[mm/s] as a function of pressure P[bar] at different propellant initial temperatures T[°C]

	-30° C	20° C	50° C
Ambient pressure	22.2	23.9	26.1
50 bars	26.4	28.8	30.3
100 bars	27	29.5	31.3
150 bars	28	30	31.7
200 bars	28.5	30.7	32.2
250 bars	28.6	31.1	32.9
300 bars	28.7	31.5	33.5
350 bars	28.8	32.1	34
400 bars	29	32.5	34.3
450 bars	29.3	33	34.5
500 bars	29.5	33.5	34.9

In order to determine the variation of burning rate as a function of pressure, experiments were conducted on the solid propellant at various working pressures and initial propellant temperatures. The scatter plot obtained presented in Table 3. is fitted using regression to establish a mathematical relationship between the burning rate (r), working pressure (P), and the adjusted coefficients (a and n) of the Saint-Robert and Vieille equation (5), defined as follows:

$$r_{20} = 23.684 \cdot P^{0.05} \tag{12}$$

Using equation (6) and data from table 4.

$$r_{T_i} = r_{20} \cdot e^{\sigma \cdot (T_i - 20)} \tag{13}$$

Where σ is the temperature sensitivity of the propellant and it is equal to 0.00175/°C.

Figure 6. presents the comparison between the predicted curves of the chamber pressure in time at different initial propellant temperatures at T = -30°C, 20°C and 50°C.

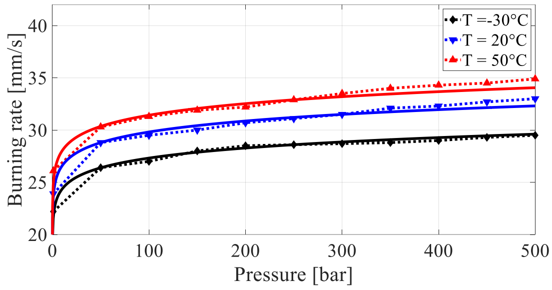

Figure 6. Burning rate at different initial propellant temperatures

For the same motor with the same propellant grain under different initial temperatures, from figure 6, there is a difference in the pressure curves. We notice that this initial propellant temperature has an effect on burning time and chamber pressure such that, the higher the initial propellant temperature, the higher-pressure chamber and lower is burning time and vice versa.

4. RESULTS AND DISCUSSION

Simulation allowed to predict the pressure-time curve for different initial propellant temperatures, results are shown in Figure 7 and 8 for the two cases of grain state (ideal and imperfect).

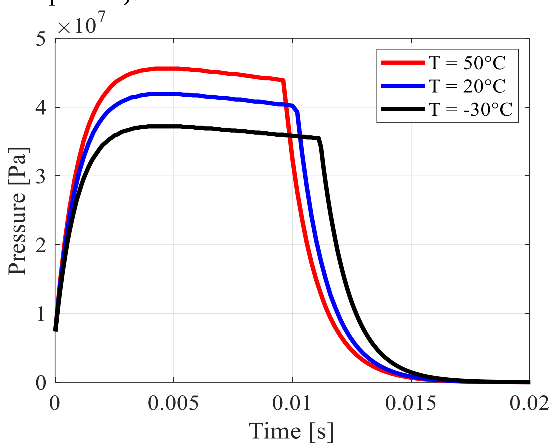

Figure 7. Predicted pressure vs. time at different temperatures for the ideal tubes.

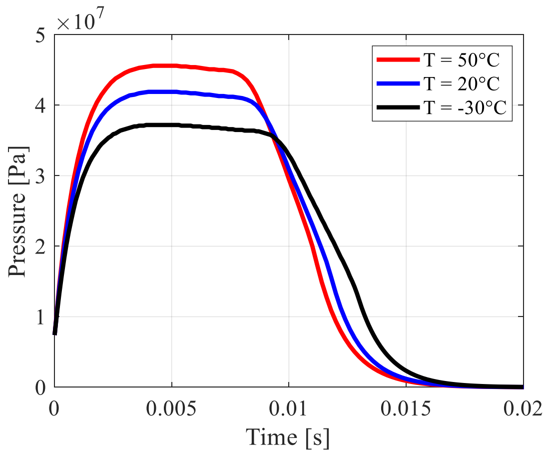

Figure 8. Predicted pressure vs. time at different temperatures for the imperfect tubes.

Comparaison between the pressure vs. Time curves of simulations of the ideal and imperfect propellant allows to see the consequences of the manufactoring imperfections on performances of the thruster.

For the ideal propellant, the curves show an uniform profile of pressure, indicating an optimal combustion process, while the curves of the imperfect propellant grain present a deviation from the standard pressure-time profile, they exhibit longer burn duration, a quite higher peak of pressure but drop and decreases faster compared to the ideal propellant. The higher peak is caused by the rapid combustion due to the imperfections, these imperfectins during combustion creates unburned fragments called *Sliver*. Slivers burn slower creating an additional burning time and this explain the longer burn duration of the imperfect propellant.

A thruster prototype is manufactured (Figure 9) and tested on the test bench described earlier in Figure 3.

The test was carried out at an initial propellant temperature of 20°C, Figure 10 presents the comparison between the analytic and the experimental curves of the chamber pressure in time.

Figure 9. The thruster prototype

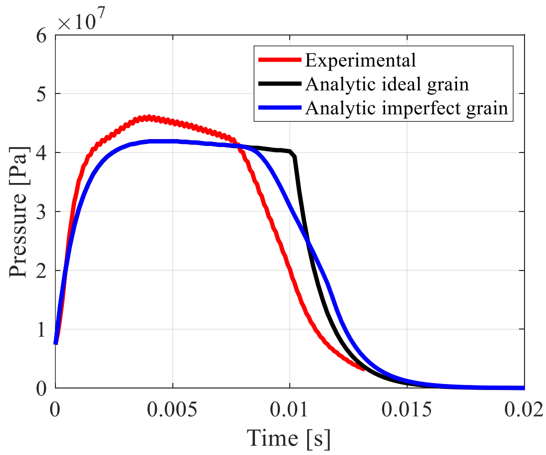

Figure 10. Predicted and experimental pressure curve versus time at 20°C

Data shows a good correspondence between the curves in terms of shape and values with a small error margins in values. The analytic curves show a constant work pressure of 418 bar, an effective working time of 10ms with an ideal propellant and 8ms with an imperfect propellant grain while the experimental curve shows higher quite constant pressure of 447 bar, it starts to decrease at t = 7.5ms.

Comparing the analytic curves with the experimental, the experimental curve is closer to the curve of the imperfect grain, this is due to the fact that the used propellant tubes presents some manufacturing imperfections (non-coaxial).

5. CONCLUSION

In this work, a lateral thruster is designed through internal ballistic calculations and rocket propulsion theory. A prototype model is manufactured and tested on a static test bench, in which the pressure-time variations is successfully measured. Results obtained by the analytic model and those obtained experimentally show a good agreement which demonstrates the reliability of the internal ballistic mathematical model of rocket motors.

The experimental approach showed that thrusters, as a rocket motor with a very short operating time, are very sensitive to many parameters which can influence their performances. From this, to design a thruster, many considerations must be carefully taken to reach the desired performances. Thrusters use a quick-burn propellant which is particularly the most sensitive parameter. Being susceptible to manufacturing imperfections, this can grossly affect the thruster performances.

Nomenclature

Latin symbols

A_b	-	Burning surface area, [m^2]
A_{th}	-	Nozzle throat area, [m^2]
a	-	Temperature constant, [-]
C_d	-	Mass flow coefficient, [-]
C_F	-	Thrust coefficient, [-]
D	-	Outer diameter of a unit propellant tube, [m]
D_e	-	Nozzle exit diameter, [m]
d	-	Inner diameter of a unit propellant tube, [m]
F	-	Thrust force, [N]
I_{sp}	-	Specific impulse, [N.s/Kg]
I_{tot}	-	Total impulse, [N.s]
L	-	Length of a unit propellant tube, [m]
m	-	Propellant mass, [Kg]
$\dot{m}$	-	Mass flow, [Kg/s]
n	-	pressure exponent, [-]
P	-	Chamber pressure, [Pa]
P_a	-	Atmospheric pressure, [Pa]
R	-	Gas constant, [J/(K.mol.K)]
r	-	Burning rate, [m/s]
r_{T_i}	-	Burning rate at T_i , [m/s]
T	-	Propellant initial temperature, [K]
T_0	-	Temperature of combustion, [K]
t	-	Time, [s]
t_e	-	Thruster effective working time, [s]
V_0	-	Free volume in the combustion chamber, [m^3]
x	-	Web, [m]

Greek symbols

κ	-	Specific heat ratio, [-]
ρ	-	Density, [Kg/m3]
σ	-	Temperature sensivity, [K^{-1}]

Acknowledgements

This work was by Serbian Ministry of Defense and Serbian Ministry of Education, Science and Technological Development, Grant No 451-03-66/2024-03/200325.

References

[1] S. Mitzer and J. Oliemans , "Oryx," [Online]. Available: https://www.oryxspioenkop.com/2021/05/novel-capabilities-ukraines-vilkha-mrl.html?m=1. [Accessed 20 02 2024].

[2] "Wikimedia," [Online]. Available: https://upload.wikimedia.org/wikipedia/commons/5/58/JASDF_MIM-104_Patriot_PAC-3_Missile%28dummy_model%29_side_thruster_at_Hamamatsu_Air_Base_October_20%2C_2019.jpg [Accessed 27 06 2024].

[3] Gupta, S.K., Saxena, S., Singhal, A. and Ghosh, A.K., «Trajectory Correction Flight Control System using Pulsejet on an Artillery Rocket,» *Defence Science Journal*, vol. 58 (1), pp. 15-33, 2008.

[4] T. Jitpraphai and M. Costello, «Dispersion Reduction of a Direct-Fire Rocket Using Lateral Pulse Jets,» *Journal of Spacecraft and Rockets*, vol. 38 (6), pp. 929-936, April 2001.

[5] R. Głebocki and M. Jacewicz , «Sensitivity Analysis and Flight Tests Results for a Vertical Cold Launch Missile System,» *Aerospace*, vol. 7(12):168, 2020.

[6] S. Živković, «Naučnotehničke informacije», Vol. LII, Br.4, Beograd, 2015.

[7] D. Kumar et al., «Design and Structural Analysis of Solid Rocket Motor Casing Hardware used in Aerospace Applications,» *Journal of Aeronautics & Aerospace Engineering*, vol. 5(2), 2016.

[8] Md Akhtar khan, B.K chaitanya and Eshwar Reddy cholleti, «Conceptual Design and Structural Analysis of Solid Rocket Motor Casing,» *International Journal of Computational Engineering Research (IJCER)*, vol. 7 (2), pp. 23-28, 2017.

[9] Zhu, L.;Wang, J.; Shen,W.; Chen, L.; Zhu, «Design and Analysis of Solid Rocket Composite Motor Case Connector Using Finite Element Method,» *Polymers*, vol. 14(13), 2022.

[10] M. ALAZEEZI, Nikola P. POPOVIĆ and Predrag M. ELEK, "Two-Component Propellant Grain For Rocket Motor Combustion Analysis And Geometric

Optimization," *Thermal Science*, vol. 26 (2B), pp. 1567-1578, 2022.

[11] Hainline, Roger, "Design Optimization Of Solid Rocket Motor Grains For Internal Ballistic Performance," University of Central Florida, Orlando, Florida, 2006.

[12] S. Veerendra Prasad, Dr. B. V. R. Ravi Kumar and Dr. V. V. Subba Rao, "Static Testing Of Solid Fuel Rocket Engine," *Journal of Engineering Sciences*, vol. 11(2), pp. 863-866, Feb 2020.

[13] F. Augusto, C. Fernandes, C. d'Andrade Souto and R. Pirk, "Static Firing Tests of Solid Propellant Rocket Motors: Uncertainty Levels of Thrust Measurements," *J. Aerosp. Technol. Manag*, 2022.

[14] Yuan, Chung-I, «An interactive computer code for preliminary design of solid propellant rocket motors,» Montery, California, 1987.

[15] R. A. Nakka, Solid Propellant Rocket Motor Design and Testing, Department of Mechanical Engineering - The Faculty of Engineering - The Univercity of Manitoba, 1984.

[16] D. Mishra, «Fundamentals of Rocket Propulsion,» Taylor & Francis Group, 2017